Received: 2 April 2024 | Revised: 22 July 2024 | Accepted: 25 July 2024

DOI: 10.1111/epi.18088

Epilepsia®

RESEARCH ARTICLE

Oscillatory and nonoscillatory sleep electroencephalographic biomarkers of the epileptic network

Véronique Latreille[1] | **Justin Corbin-Lapointe**[2] | **Laure Peter-Derex**[3] | **John Thomas**[4] | **Jean-Marc Lina**[2] | **Birgit Frauscher**[1,4]

[1]Department of Neurology and Neurosurgery, Montreal Neurological Institute–Hospital, McGill University, Montreal, Quebec, Canada

[2]Department of Electrical Engineering, École de Technologie Supérieure, Montreal, Quebec, Canada

[3]Center for Sleep Medicine, Croix-Rousse Hospital, Lyon University Hospital, Lyon, France

[4]Department of Neurology, Analytical Neurophysiology Lab, Duke University, Durham, North Carolina, USA

Correspondence
Birgit Frauscher, Department of Neurology, Duke University, Durham, NC, 27710, USA.
Email: birgit.frauscher@duke.edu

Funding information
Canadian Institutes of Health Research, Grant/Award Number: PJT-175056; Banting Postdoctoral Fellowship 2020–2023; Fonds de Recherche du Québec–Santé: Salary Award Chercheur-Boursier Clinicien Senior 2021–2023

Abstract

Objective: In addition to the oscillatory brain activity, the nonoscillatory (scale-free) components of the background electroencephalogram (EEG) may provide further information about the complexity of the underlying neuronal network. As epilepsy is considered a network disease, such scale-free metrics might help to delineate the epileptic network. Here, we performed an analysis of the sleep oscillatory (spindle, slow wave, and rhythmic spectral power) and nonoscillatory (*H* exponent) intracranial EEG using multiple interictal features to estimate whether and how they deviate from normalcy in 38 adults with drug-resistant epilepsy.

Methods: To quantify intracranial EEG abnormalities within and outside the seizure onset areas, patients' values were adjusted based on normative maps derived from the open-access Montreal Neurological Institute open iEEG Atlas. In a subset of 29 patients who underwent resective surgery, we estimated the predictive value of these features to identify the epileptogenic zone in those with a good postsurgical outcome.

Results: We found that distinct sleep oscillatory and nonoscillatory metrics behave differently across the epileptic network, with the strongest differences observed for (1) a reduction in spindle activity (spindle rates and rhythmic sigma power in the 10–16 Hz band), (2) a higher rhythmic gamma power (30–80 Hz), and (3) a higher *H* exponent (steeper $1/f$ slope). As expected, epileptic spikes were also highest in the seizure onset areas. Furthermore, in surgical patients, the *H* exponent achieved the highest performance (balanced accuracy of .76) for classifying resected versus nonresected channels in good outcome patients.

Significance: This work suggests that nonoscillatory components of the intracranial EEG signal could serve as promising interictal sleep candidates of epileptogenicity in patients with drug-resistant epilepsy. Our findings further advance the understanding of epilepsy as a disease, whereby absence or loss of sleep physiology may provide information complementary to pathological epileptic processes.

KEYWORDS

epilepsy, scale-free, sleep oscillations, stereo-electroencephalography

1 | INTRODUCTION

In patients with focal drug-resistant epilepsy, surgery is the treatment of choice,[1,2] but accurate identification of the precise surgical target is crucial.[3] Over the past decade, multiple research groups have identified and tested various promising biomarkers for the epileptogenic zone (EZ), including among others, high-frequency oscillations (80–250 Hz),[4] specific epileptic spike features,[4,5] and a combination of multiple interictal features.[6] Non-rapid eye movement (NREM) sleep was found to be the best state of vigilance for capturing the essential interictal information related to the EZ.[6] Despite these developments, the success of epilepsy surgery stagnates at approximately 50%.[4]

NREM sleep electroencephalogram (EEG) is characterized on the one hand by specific oscillatory patterns, including sleep spindles (10–16 Hz waxing and waning bursts) and slow waves (SWs; high-amplitude waves, <4 Hz), and on the other hand by nonoscillatory (arrhythmic) patterns reflecting the background neuronal activity. Accumulating evidence indicates that spindles and SWs are associated with epileptic activity,[7–9] and spindles more particularly also have a localizing value for epileptic regions.[10–12] Yet more investigation is needed to better define the potential role of these sleep oscillations in localizing the epileptic network. In addition to the oscillatory brain activity, the nonoscillatory (scale-free) components of the EEG may provide further information about the complexity of the underlying neuronal network. Recent work suggests that scale-free activity may reflect the local cortical excitatory–inhibitory balance,[13] which is relevant when studying abnormal epileptic networks.[14]

Scale-free EEG activity can be quantified using different metrics, such as "$1/f^{\beta}$ spectrum"[15]—where β refers to a unique scaling exponent (monofractal)—a metric that has been applied to epilepsy.[16–18] However, the complexity of the EEG signal cannot be fully considered in a monofractal model, because scaling exponents vary with time, resulting in multiple scaling exponents (multifractal systems), as demonstrated with scalp or stereo-EEG (SEEG) data in epilepsy patients.[19,20] Using such a multifractal approach, we previously showed that the use of a scale-free metric (H exponent) could predict seizure occurrence in patients with mesial temporal lobe epilepsy.[21] Yet it is unknown whether the H exponent can help delineate the epileptic network using interictal SEEG sleep recordings. It is worth mentioning that the arrhythmic activity is a ubiquitous background always available for quantification, in contrast to sporadically occurring sleep spindles and SWs, and even interictal epileptic spikes, and therefore might be more informative for identifying the EZ. To our knowledge, a comprehensive investigation of both rhythmic activities (mostly represented with sleep spindles and SWs) and the arrhythmic background (characterized by the scale-free exponent) has not been performed in the context of epilepsy.

Key points

- Specific NREM sleep oscillatory and nonoscillatory brain activity features are altered by the epileptic network.
- Relative to non-SOZ areas, the SOZ exhibited reduced spindle activity, higher rhythmic gamma power, and scale-free H exponent during N2 sleep.
- The H exponent metric performed best for classifying resected versus nonresected channels in patients with good postsurgical outcomes.
- Scale-free metrics constitute promising interictal sleep biomarkers of the SOZ in patients with drug-resistant epilepsy.
- This current work adds support to the absence of physiology as an interesting and promising direction for epilepsy research.

As a first step, we analyzed sleep oscillatory and nonoscillatory brain activity patterns using multiple SEEG features to delineate the clinical seizure onset zone (SOZ) from non-SOZ areas of focal drug-resistant epilepsy patients. We used a normative modeling approach to estimate whether and how these specific brain features deviate from normalcy and whether these could serve as potential markers of the EZ. In the subset of patients who underwent resective surgery, we further estimated the predictive value of our features as biomarkers of the EZ in those with a good postsurgical outcome.

2 | MATERIALS AND METHODS

2.1 | Participants

Simultaneous scalp–intracranial EEG data from 38 consecutive patients with drug-resistant epilepsy (mean

age = 34.4 ± 10.8 years, age range = 18–61 years, 20 women) who underwent SEEG monitoring at the Montreal Neurological Institute–Hospital (MNI) between March 2010 and January 2020 as part of their presurgical evaluation were selected. Patient selection criteria and detailed patient information are provided in the Supplementary Material. A schematic of the study design is provided in Figure 1. This study was approved by the MNI Research Ethics Board.

2.2 | Recordings

SEEG exploration was performed using multicontact depth macroelectrodes implanted stereotactically at positions tailored for each individual subject, depending on the clinical hypothesis. Anatomical localization of electrodes was determined as done in our previous research.[24] Recordings were acquired using Harmonie software (Stellate Systems) or NeuroWorkbench software (Nihon

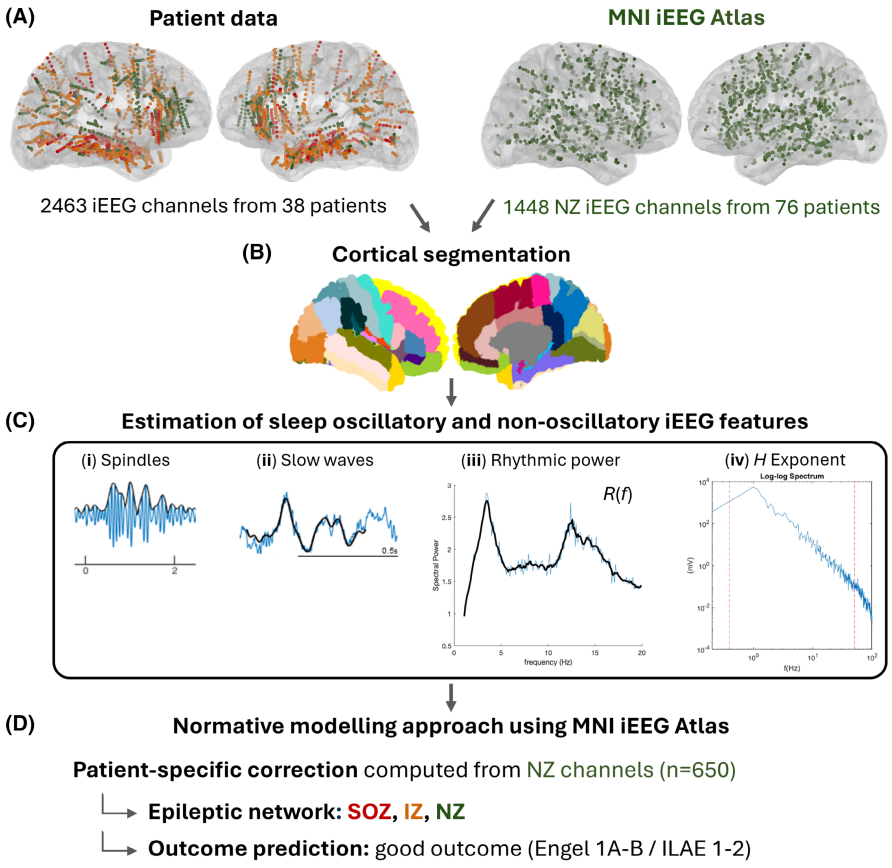

FIGURE 1 Schematic of study design. (A) We analyzed stereo-electroencephalographic (SEEG) data of 38 patients with drug-resistant focal epilepsy implanted with depth electrodes ($n = 2463$ bipolar channels). To quantify SEEG abnormalities within the epileptic network, we used a normative modeling approach derived from an open-access intracranial sleep electroencephalographic atlas (Montreal Neurological Institute open iEEG Atlas [MNI open intracranial EEG Atlas],[22] $n = 1448$ bipolar channels from 76 patients). (B) Data from patients and from the MNI open iEEG Atlas were computed following the same procedures; all bipolar SEEG channels were assigned to their respective brain region ($n = 38$ cortical areas, derived from the MICCAI 2012 atlas[23]). (C) We then estimated several oscillatory and nonoscillatory features during early non-rapid eye movement sleep (N2 and N3 sleep): (i) spindles, (ii) slow waves, (iii) residual rhythmic spectral power in multiple frequency bands (delta .5–4 Hz, theta 4–8 Hz, sigma 10–16 Hz, beta 13–30 Hz, and gamma 30–80 Hz), and (iv) the scale-free H exponent. (D) For each feature, we obtained the mean value of each normal cortical region (normal zone [NZ] channels) and estimated for each patient how much a given value deviates from the normative atlas (in the homologous region). We then applied a patient-specific correction to estimate the sleep features in the remaining cortical regions to obtain values for the seizure onset zone (SOZ) and irritative zone (IZ). Using a within-subject design, we compared each feature across the epileptic network: (i) SOZ ($n = 499$ channels), (ii) IZ ($n = 1314$ channels), and (iii) NZ ($n = 650$ channels). Finally, we estimated the predictive value of the sleep features as biomarkers of the epileptogenic zone in a subset of 29 patients who underwent resective surgery and tested our model in 13 good outcome patients (Engel IA–B and International League Against Epilepsy [ILAE] scores 1–2).

Kohden) and sampled at 2000 Hz, with a high-pass filter at .1 Hz and a low-pass filter at 500 Hz (Stellate Systems) or 600 Hz (Nihon Kohden). For all analyses, the recordings were downsampled to 200 Hz for direct comparison to the Montreal Neurological Institute open iEEG Atlas. Nine subdermal electrodes (frontal, central, and parietal) were placed at the time of implantation for scalp recording and sleep scoring. For analysis of SEEG metrics, following inspection of scalp and SEEG channels, we visually selected the first 10 min of artifact-free N2 and N3 sleep from the first sleep cycle, given that SWs and spindles are predominant in the first part of the night.[25] For cases where N3 sleep was either absent or too short (<2 min) during the first sleep cycle, additional epochs were selected from the beginning of the second sleep cycle.

2.3 | Selection of the seizure onset, irritative, and normal zones

For each subject, SEEG channels were grouped within three clinically defined zones: (1) SOZ: channels showing the first unequivocal ictal SEEG change at seizure onset independent of the frequency content[26]; (2) irritative zone (IZ): channels showing epileptic spikes but localized outside the SOZ; and (3) normal zone (NZ): channels showing "normal" physiological activity, with no or only very rare epileptiform abnormalities and not localized within lesional areas based on magnetic resonance imaging. Channels localized outside the gray matter or those displaying nonepileptic abnormalities were excluded. Selection of SEEG channels within each zone of interest was performed by board-certified electrophysiologists based on careful review of the recordings from the entire SEEG implantation period.

2.4 | Definition of the EZ and outcome prediction

SEEG channels were defined as resected or nonresected by overlaying the electrode contact locations derived from the peri-implantation and postsurgical scans. In good outcome patients, the resection cavity contains the EZ. For these cases, it is reasonable to assume that the resection approximates the EZ ± a small percentage of normal tissue which resection was required to reach the EZ. In contrast, in the poor outcome group, the resection cavity contains only part or no tissue belonging to the "true" EZ, given that otherwise the surgery should have achieved seizure freedom in these patients. To avoid any a priori assumptions, we used the terms resected and nonresected throughout. Outcome of epilepsy surgery was evaluated at >1 year follow-up using Engel classes[27] and International League Against Epilepsy (ILAE) scores[28]; good outcome was defined as Engel class IA–IB and ILAE scores 1–2, whereas seizure recurrence was defined as Engel classes IC–IV+ and ILAE scores 3–5.

2.5 | Data processing

2.5.1 | Epileptic spike detection

Epileptic spikes were detected automatically on SEEG channels during NREM sleep epochs using a validated algorithm,[29] as done in our previous works.[30,31] For each subject, we quantified the total number of spikes per minute for all channels and then normalized it to the total number of channels analyzed within the SOZ, IZ, and NZ to obtain a single value per zone.

2.5.2 | Oscillatory brain activity

Spindles and SWs were automatically detected on SEEG channels during NREM sleep using previously published methods,[32,33] which have been applied to SEEG data.[22,34] For more details of the sleep spindle and SW event detection algorithm, please see further information in the Supplementary Material. For each subject, we quantified the rate of detected spindles and SWs for all channels during N2 and N3 sleep.

Next, we computed the "rhythmic spectral power" from frequency bands of interest, which isolates the oscillatory components of the signal from the nonoscillatory scale-free activity (see Figure S1 in the Supplementary Material). For each 20-s page subdivided into 4-s epochs (with 1-s overlap), we first estimated the exponent β of the $1/f$ slope from the log–log Welch power spectrum. Writing the epochwise power spectrum as $P(f) = c/f\hat{}\beta\ R(f)$, the residual power $R(f)$ reflects the rhythmic component of the signal. We then averaged all the factors $R(f)$ across N2 and N3 sleep segments. We analyzed the rhythmic power in the .25–250-Hz range and broke down the frequency bands as follows: delta (.5–4 Hz), theta (4–8 Hz), sigma (10–16 Hz), beta (13–30 Hz), and gamma (30–80 Hz), taking the mean value within each band.

2.5.3 | Nonoscillatory brain activity

The scale-free component of the SEEG signal was determined by computing the H exponent (also called Hurst or Hölder exponent) as well as its dispersion (D) using the open-source Wavelet Leaders and Bootstrap

to Multifractal Formalism MATLAB toolbox (https://www.irit.fr/~Herwig.Wendt/software.html). The H exponent reflects the fractal dimension of the signal and characterizes the steepness of the $1/f^{\beta}$ background of the spectrum, where β refers to a characteristic scaling exponent (see Figure S1 in the Supplementary Material). A greater H exponent reflects a steeper slope. Because H may not be unique along the analyzed time series, we applied the wavelet-leaders formalism to estimate the local and most prevalent H exponent derived over all possible values of H.[35,36] The scaling exponent is computed by $\beta = 2H + 1$. An H exponent of >.5 corresponds to a persistent (regular) signal, whereas an H exponent of <.5 corresponds to an antipersistent (irregular) one. The D provides information about the spread of the distribution of the H exponent. This is commonly represented in the log–log plot of the $1/f$ spectrum as a "knee," indicating that the signal is multifractal, and will have a greater absolute D value. By contrast, a signal that is more regular across time scales will have a D closer to 0 (monofractal signal). Data segments were excluded if the multifractal model was deemed illegitimate based on its distribution, and therefore we excluded data points with a negative D value. To investigate the difference in scale-free activity across the SOZ, IZ, and NZ, we quantified the H metric for every artifact-free 20-s epoch of N2 and N3 sleep segments.

2.6 | Normalization to the Montreal Neurological Institute open iEEG Atlas

As previously demonstrated using the Montreal Neurological Institute open iEEG Atlas,[22] physiological sleep spindles and SWs exhibit specific cortical patterns, with lower rates in the medial temporal areas. Given that the temporal lobes are frequent sites of epileptogenicity, we wished to account for potential topographic and epilepsy localization effects on the oscillatory and nonoscillatory metrics of interest. Therefore, we leveraged the availability of the Montreal Neurological Institute open iEEG Atlas (available at https://mni-open-ieegatlas.research.mcgill.ca)[22] to quantify SEEG abnormalities across the brain and estimate how much a given value deviates from normalcy. Detailed information on the normalization steps is provided in the Supplementary Material.

2.7 | Statistical analysis

Shapiro–Wilk tests were performed for testing the normality of data. SWs, rhythmic power variables, the H exponent ratio, and spike rates were not normally distributed. For these variables, we used nonparametric tests, but untransformed data are presented in the Figures. At the group level, we compared the oscillatory and nonoscillatory metrics across the three zones of interest during NREM sleep using two-way repeated measures analyses of variance with sleep stages (N2, N3) and zones (SOZ, IZ, and NZ) as independent factors. Post hoc comparisons were performed and adjusted with Bonferroni correction. Nonparametric Friedman and Wilcoxon tests were performed for variables not normally distributed. Effect sizes are reported for each analysis. We also performed Spearman correlations between the oscillatory and nonoscillatory variables and epileptic spike rates within the SOZ.

In the subset of surgical patients ($n = 29$), we then tested whether some of the oscillatory and nonoscillatory metrics differed between the resected and nonresected channels among those with good outcomes, as well as between the resected and nonresected channels in those with poor outcomes using nonparametric Mann–Whitney U-tests. Next, we estimated the predictive value of the sleep features as potential biomarkers of the EZ by calculating the (1) area under the receiving operating characteristic curve (AUC); (2) area under the precision–recall curve; and (3) balanced accuracy (BAC), defined as the mean of sensitivity and specificity values. The performance measures were computed by using the resected channels as the ground truth. Given the unbalanced number of resected and nonresected channels, to prevent bias in the data, we calculated these prediction values for each individual good outcome patient as well as the group average. As a benchmark, we compared the BAC values of our features to those obtained in SOZ channels (expressed as a binary variable).

3 | RESULTS

3.1 | Specific sleep oscillatory components are altered by the SOZ

As depicted in Figure 2A,B, spindle but not SW rates differed across the epileptic network during NREM sleep. Post hoc comparisons with Bonferroni correction revealed that spindle rates were significantly lower in the SOZ relative to the IZ and NZ, as well as between the IZ and NZ during N2 and N3 sleep (Figure 2A). In contrast, SW rates were slightly higher in the SOZ than the NZ during N2 sleep, although p-values of post hoc comparisons did not survive Bonferroni correction ($p > .003$; Figure 2B). As expected, epileptic spike rates were highest in the SOZ relative to both the IZ and NZ, as well as between the IZ and NZ during N2 and N3 sleep (Figure 2C).

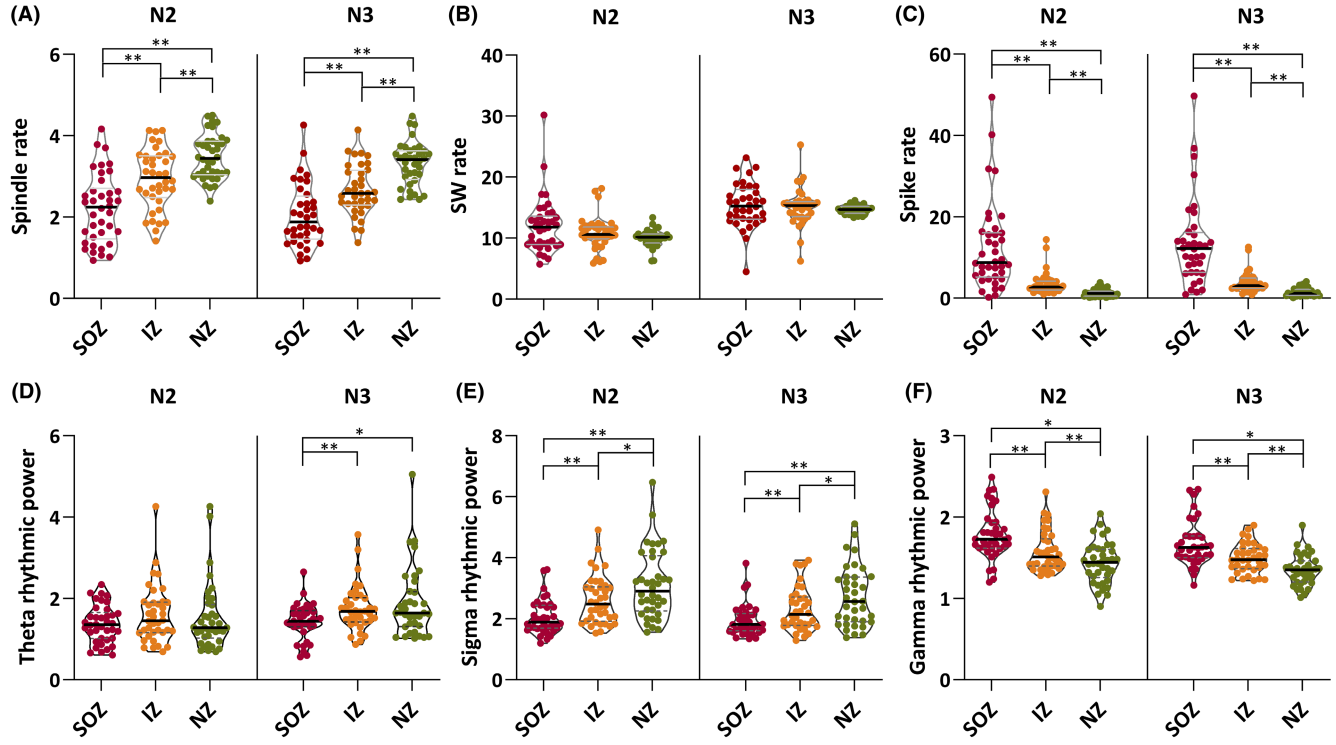

FIGURE 2 Specific oscillatory metrics distinguish the seizure onset zone (SOZ) from non-SOZ areas during non-rapid eye movement sleep. (A) Spindle rates are lower in the SOZ during N2 (analysis of variance [ANOVA] of main effect of zones: $F[2, 74] = 38.34$, $p < .001$, effect size = .51) and N3 sleep (ANOVA main effect of zones: $F[2, 74] = 41.95$, $p < .001$, effect size = .55). Post hoc comparisons with Bonferroni adjustment revealed differences between the SOZ and irritative zone (IZ; $p < .001$, N2 effect size = .77, N3 effect size = .75) and normal zone (NZ; $p < .001$, N2 effect size = 1.05, N3 effect size = .96), as well as between the IZ and the NZ ($p < .001$, N2 effect size = .84, N3 effect size = .76). (B) Physiologic slow wave (SW) rates are higher in the SOZ during N2 sleep (Friedman test: $\chi^2[2] = 14.58$, $p < .001$, effect size = .39), although post hoc comparisons did not survive the Bonferroni correction set at $p < .003$. (C) Epileptic spike rates significantly differed across the epileptic network during N2 (Friedman test: $\chi^2[2] = 5.11$, $p < .001$, effect size = 1.35) and N3 sleep (Friedman test: $\chi^2[2] = 45.17$, $p < .001$, effect size = 1.29). Post hoc comparisons with Bonferroni adjustment revealed differences between the SOZ and IZ ($p < .001$, N2 effect size = .79, N3 effect size = .80) and NZ ($p < .001$, N2 effect size = .84, N3 effect size = .83), as well as between the IZ and the NZ ($p < .001$, N2 effect size = .82, N3 effect size = .76). (D) A main effect of zone was observed for theta rhythmic power during N3 sleep only (Friedman test: $\chi^2[2] = 18.39$, $p = .001$, effect size = .53). Wilcoxon post hoc comparisons showed lower residual theta power in the SOZ relative to the IZ ($p < .001$, effect size = .74) and NZ ($p = .001$, effect size = .56). (E) Rhythmic power in the sigma band showed statistically significant effect of zones during N2 (Friedman test: $\chi^2[2] = 33.53$, $p < .001$, effect size = .91) and N3 sleep (Friedman test: $\chi^2[2] = 28.17$, $p < .001$, effect size = .81). Wilcoxon post hoc comparisons revealed lower residual sigma power in the SOZ and the IZ ($p < .001$, N2 effect size = .77, N3 effect size = .62) and NZ ($p < .001$, N2 effect size = .79, N3 effect size = .74), as well as lower residual sigma power in the IZ relative to the NZ ($p < .001$, N2 effect size = .58, N3 effect size = .54). (F) Rhythmic gamma power showed statistically significant effect of zones in N2 (Friedman test: $\chi^2[2] = 39.79$, $p < .001$, effect size = 1.08) and N3 sleep (Friedman test: $\chi^2[2] = 40.50$, $p < .001$, effect size = 1.16). Post hoc comparisons revealed differences between all three zones, with higher residual gamma power in the SOZ versus IZ ($p < .001$, N2 effect size = .74, N3 effect size = .67) and NZ ($p < .001$, N2 effect size = .78, N3 effect size = .76), and in the IZ relative to the NZ ($p < .001$, N2 effect size = .56, N3 effect size = .80). Asterisks indicate post hoc contrasts with significant differences (*$p < .003$, **$p < .001$). Black thick lines in violin plots represent the median; gray lines represent the quartiles.

For rhythmic spectral analyses, we found significant interactions between the zones and stages of sleep for all frequency bands except the gamma band, and therefore examined the main effects of zones for N2 and N3 sleep separately for the following analyses. Rhythmic power in the theta, sigma, and gamma bands significantly differed across the zones during N2 and/or N3 sleep (Figure 2D–F). No significant differences in rhythmic delta and beta power were found between the zones following Bonferroni correction (data not shown). Residual rhythmic power in the theta band showed effects that were specific to N3 sleep, with lower power in the SOZ relative to the IZ and NZ (Figure 2D). During N2 and N3 sleep, rhythmic power in the sigma band differed between zones; power was lower in the SOZ relative to the IZ and NZ, as well as in the IZ compared to the NZ (Figure 2E). In contrast, residual power in the gamma range was higher in the SOZ relative to the NZ during both sleep

TABLE 1 Predictive values of oscillatory and nonoscillatory metrics to identify the resected channels in good outcome patients.

Patient ID	*H* exponent ratio			*H* exponent N2			SOZ[a]	Spike rate N2		
	BAC	AUC	AUPRC	BAC	AUC	AUPRC	BAC	BAC	AUC	AUPRC
2	.895	.950	.845	.865	.895	.659	.860	.733	.667	.273
10	.875	.850	.326	.896	.862	.340	.552	.573	.491	.136
25	.856	.909	.652	.898	.928	.616	.667	.855	.788	.646
34	.829	.898	.791	.667	.581	.327	.900	.858	.879	.862
35	.827	.865	.659	.780	.847	.805	.921	.868	.896	.787
1	.813	.861	.605	.810	.711	.567	.975	.946	.964	.886
4	.732	.656	.296	.706	.730	.505	.836	.684	.715	.587
13	.721	.777	.659	.781	.824	.588	.671	.638	.637	.316
11	.714	.602	.067	.694	.707	.392	.959	.650	.548	.068
20	.701	.705	.385	.667	.666	.430	.434	.691	.546	.188
33	.695	.591	.058	.836	.870	.217	.943	.623	.451	.066
22	.693	.636	.207	.604	.523	.251	.657	.667	.694	.505
24	.668	.628	.213	.770	.803	.596	.493	.783	.688	.298
Mean	**.771**	**.764**	**.443**	**.767**	**.765**	**.484**	**.759**	**.736**	**.690**	**.432**

Note: Values obtained from 13 good outcome patients (total $n = 163$ resected channels; $n = 724$ nonresected channels). Balanced accuracy is the mean of sensitivity and specificity. Bold values represent the mean predictive values across all patients.

Abbreviations: AUC, area under the receiver operating characteristic curve; AUPRC, area under the precision–recall curve; BAC, balanced accuracy; SOZ, seizure onset zone.

[a]Given that the SOZ is expressed as a binary variable, only the balanced accuracy can be computed.

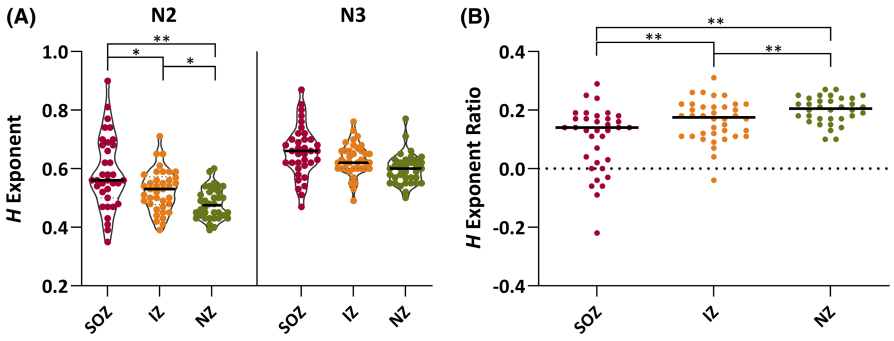

FIGURE 3 The *H* exponent distinguishes the seizure onset zone (SOZ) during N2 sleep. (A) The *H* exponent differs across the epileptic network during N2 sleep only ($F[2, 64] = 14.53$, $p < .001$, effect size = .31). Post hoc comparisons with Bonferroni adjustment revealed differences between all three zones, with higher *H* values in the SOZ versus the irritative zone (IZ; $p = .001$, effect size = .52) and normal zone (NZ; $p = .001$, effect size = .56), and higher *H* exponent in the IZ relative to the NZ ($p = .001$, effect size = .55). *H* exponent values were higher in N3 than N2 sleep ($F[1, 30] = 159.68$, $p < .001$, effect size = .84). (B) To emphasize the differences between N2 and N3 sleep, we computed a relative ratio ([N3 − N2] / N3) of the *H* exponent for each patient, and found significant differences across the epileptic network (Friedman test: $\chi^2[2] = 37.36$, $p < .001$, effect size = 1.0), with the SOZ exhibiting a lower *H* ratio during N3 over N2 sleep relative to the IZ ($p < .001$, effect size = .72) and NZ ($p < .001$, effect size = .68), and between the IZ and NZ ($p < .001$, effect size = .61). A ratio closer to zero reflects less variability between N3 and N2 sleep. Asterisks indicate post hoc contrasts with significant differences (*$p \leq .01$, **$p \leq .001$). Black thick lines in violin and scatter dot plots represent the median; gray dotted lines represent the quartiles.

stages, and also differentiated the IZ from the other two zones (Figure 2F).

Spearman correlations between the sleep metrics and spike rates in the SOZ revealed significant negative correlations for spindle rates during N2 sleep ($r = -.65$, $p < .001$) and rhythmic theta power during N3 sleep ($r = -.47$, $p = .004$). No significant correlation was found between SOZ spike rate and N3 SW rate ($r = -.21$, $p = .23$), N2 rhythmic sigma power ($r = -.04$, $p = .82$), and N2 rhythmic gamma power ($r = .25$, $p = .13$).

Spindle rate N2			Spike rate N3			Rhythmic gamma N2			Rhythmic sigma N2		
BAC	AUC	AUPRC	BAC	AUC	AUPRC	BAC	AUC	AUPRC	BAC	AUC	AUPRC
.749	.676	.314	.626	.610	.252	.772	.753	.357	.608	.569	.308
.719	.704	.209	.604	.520	.135	.781	.785	.557	.844	.764	.254
.697	.692	.394	.872	.809	.679	.630	.524	.132	.597	.573	.254
.833	.856	.759	.908	.883	.852	.650	.658	.526	.592	.440	.253
.757	.781	.704	.912	.916	.817	.636	.619	.510	.731	.669	.574
.611	.626	.243	.946	.980	.905	.917	.939	.637	.875	.874	.404
.695	.719	.616	.654	.661	.506	.658	.572	.248	.645	.614	.300
.679	.639	.360	.583	.544	.272	.651	.573	.272	.748	.742	.444
.908	.850	.147	.741	.741	.132	.837	.810	.130	.929	.918	.251
.683	.685	.276	.623	.511	.177	.603	.576	.211	.668	.685	.384
.844	.816	.123	.651	.623	.090	.681	.536	.053	.745	.759	.304
.688	.670	.292	.669	.691	.501	.644	.640	.312	.589	.566	.236
.599	.461	.149	.539	.512	.486	.750	.724	.634	.536	.428	.143
.728	**.706**	**.353**	**.718**	**.692**	**.446**	**.708**	**.670**	**.352**	**.700**	**.662**	**.316**

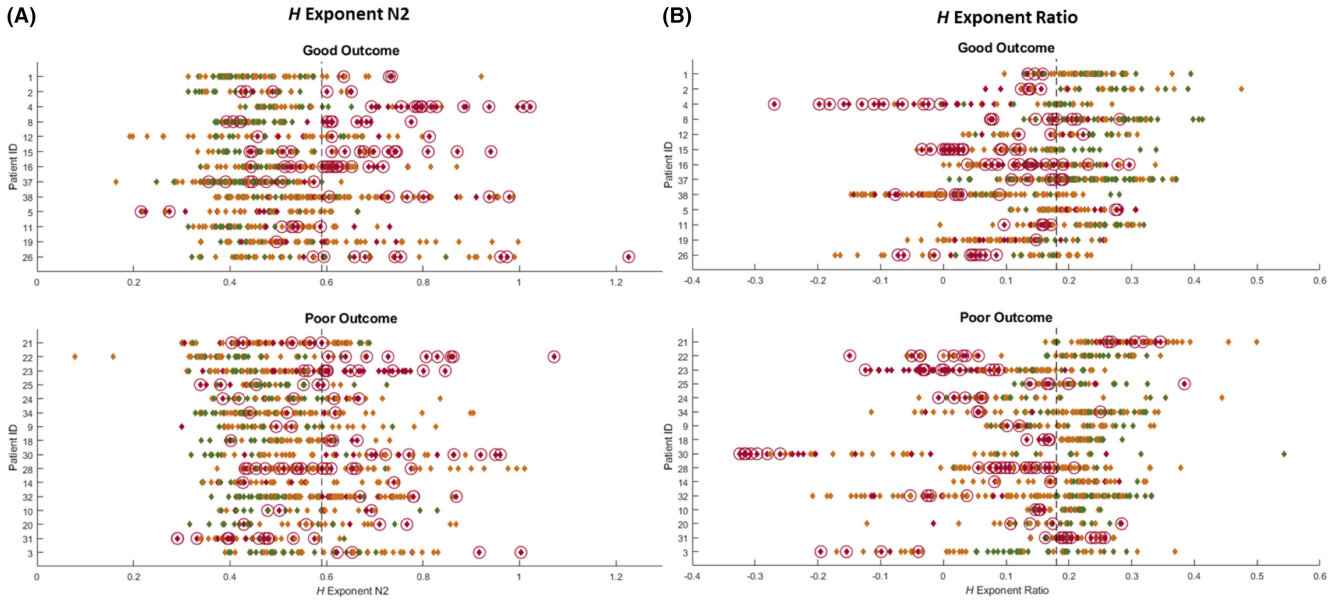

FIGURE 4 The *H* exponent metrics can help identify abnormal nonoscillatory brain activity in good outcome patients. (A) *H* exponent in N2 sleep in good outcome (top) and poor outcome patients (bottom). (B) *H* exponent ratio in good outcome (top) and poor outcome patients (bottom). Each row shows individual patient channels (represented by diamonds), classified within the seizure onset zone (red), irritative zone (orange), or normal zone (green). Patients were grouped according to their postsurgical status (Engel score). Circled diamonds represent the resected channels. Particularly in the good outcome patients, most of the SOZ channels that were also resected displayed "abnormal" *H* exponent values (highest in N2 sleep and lowest N3/N2 sleep ratios), whereas most of the NZ channels showed more "normal" *H* values. Vertical dashed lines represent the median.

3.2 | Nonoscillatory brain activity during N2 sleep distinguishes the SOZ

The *H* exponent significantly differed across the zones during N2 sleep. As depicted in Figure 3A, we found higher *H* values in the SOZ compared to both the IZ and NZ, and higher *H* exponent in the IZ relative to the NZ. The *H* exponent during N2 sleep was positively associated with spike rate ($r = .41$, $p = .01$). We also found a strong main effect of sleep stages, with *H* exponent values higher in N3 than N2 sleep (mean ± SD = .63 ± .07 vs. .53 ± .10). To emphasize the differences between the two sleep stages, we computed a relative ratio ([N3 − N2] / N3) of the *H* exponent for each patient. Post hoc comparisons revealed significant differences across the zones, with the SOZ showing a lower *H* ratio during N3 over N2 sleep compared to both the IZ and NZ and between the IZ and NZ (Figure 3B). Here, a lower *H* ratio or one that is closer to zero indicates that the *H* exponent varies less between N2 and N3 sleep.

3.3 | Predicting the EZ in good outcome patients

Among the study population, 29 patients underwent subsequent resective surgery with at least 1 year of follow-up (mean = 7.4 years, range = 2–13 years). Postoperatively, 13 patients were considered good outcome patients (Engel class IA–IB/ILAE score 1–2). Overall, we found that the best features to identify the resected channels in good outcome patients were the *H* exponent during N2 sleep as well as the H exponent ratio, achieving mean BAC and AUC values of .77 (Table 1). The *H* metrics therefore perform at least as well as the clinical SOZ, which achieved a balanced accuracy of .76. Individual patient data of the *H* exponent metrics are illustrated in Figure 4, showing that in the good outcome patients, most of the SOZ channels that were resected displayed "abnormal" *H* exponent values (highest in N2 sleep and lowest N2/N3 sleep ratios). Finally, we tested whether the features differed among good and poor outcome patients. Mann–Whitney *U*-tests revealed significant differences between the resected and nonresected channels for all N2 sleep metrics in the good outcome patients (Figure 5A–F). Effect sizes were overall largest in the good outcome patients. In the poor outcome patients, only the *H* exponent metrics and the spike rates differed among the resected and nonresected channels.

4 | DISCUSSION

In this work, we investigated the entire complexity of the sleeping brain's electrical signal, comprising both its oscillatory and nonoscillatory components, to better understand the functioning of neuronal activity during sleep and how it is altered by the epileptic process. We found that distinct NREM sleep oscillatory and nonoscillatory metrics behave differently within the SOZ relative to non-SOZ areas, with the strongest differences observed for (1) a reduction in spindle activity (spindle rates and rhythmic sigma power in the 10–16 Hz band), (2) higher rhythmic gamma power (30–80 Hz), and (3) a higher *H* exponent (steeper 1/*f* slope). Furthermore, in surgical patients, the *H* exponent achieved the highest performance for classifying resected and nonresected channels in those with good outcomes. Our findings suggest that these metrics constitute promising interictal SEEG sleep biomarkers of epileptogenicity in patients with drug-resistant epilepsy, complementing the existing biomarkers that are heavily weighted toward the presence of abnormal pathological EEG activities.[37] This current work adds support to the absence of physiology as an interesting and promising direction that was introduced more recently and evidenced from a few studies quantifying the power spectra distribution across wakefulness.[38,39]

4.1 | Specific oscillatory brain patterns are affected by the epileptic network

We observed that specific interictal oscillatory brain activities behave differently in the SOZ relative to non-SOZ areas during NREM sleep. First, we found a reduction in spindle activity in the SOZ during N2 and N3 sleep, as measured by the spindle rate and the rhythmic sigma power. The IZ also displayed lower spindle activities relative to the NZ. Although the "rhythmic spectral power" is a relatively new measure in the literature, our data show that both the spindle rates and the rhythmic sigma power provide congruent information about the oscillatory spindle activity during sleep and moderately correlate with each other ($r = .60$, $p < .001$). These findings are also in agreement with previous work from our group and others suggesting that scalp or intracranial spindles may have a localizing role regarding epileptogenicity.[10–12,40] In contrast, Clemens and Ménes[41] found higher sigma power in the epileptic hemisphere compared to the unaffected one in 20 of 27 focal epilepsy patients. However, this study was performed during N2 sleep following sleep deprivation as part of EEG activation procedures, and thus results may not reflect habitual sleep conditions and homeostasis. Furthermore, we found that spindle rates were negatively associated with epileptic spike rates within the SOZ, a result that aligns with previous studies.[12] Surprisingly, rhythmic sigma power did not show this correlation with epileptic activity. Although we excluded co-occurring spindles–spikes, we did not exclude the spikes for the rhythmic power analysis. Whether this

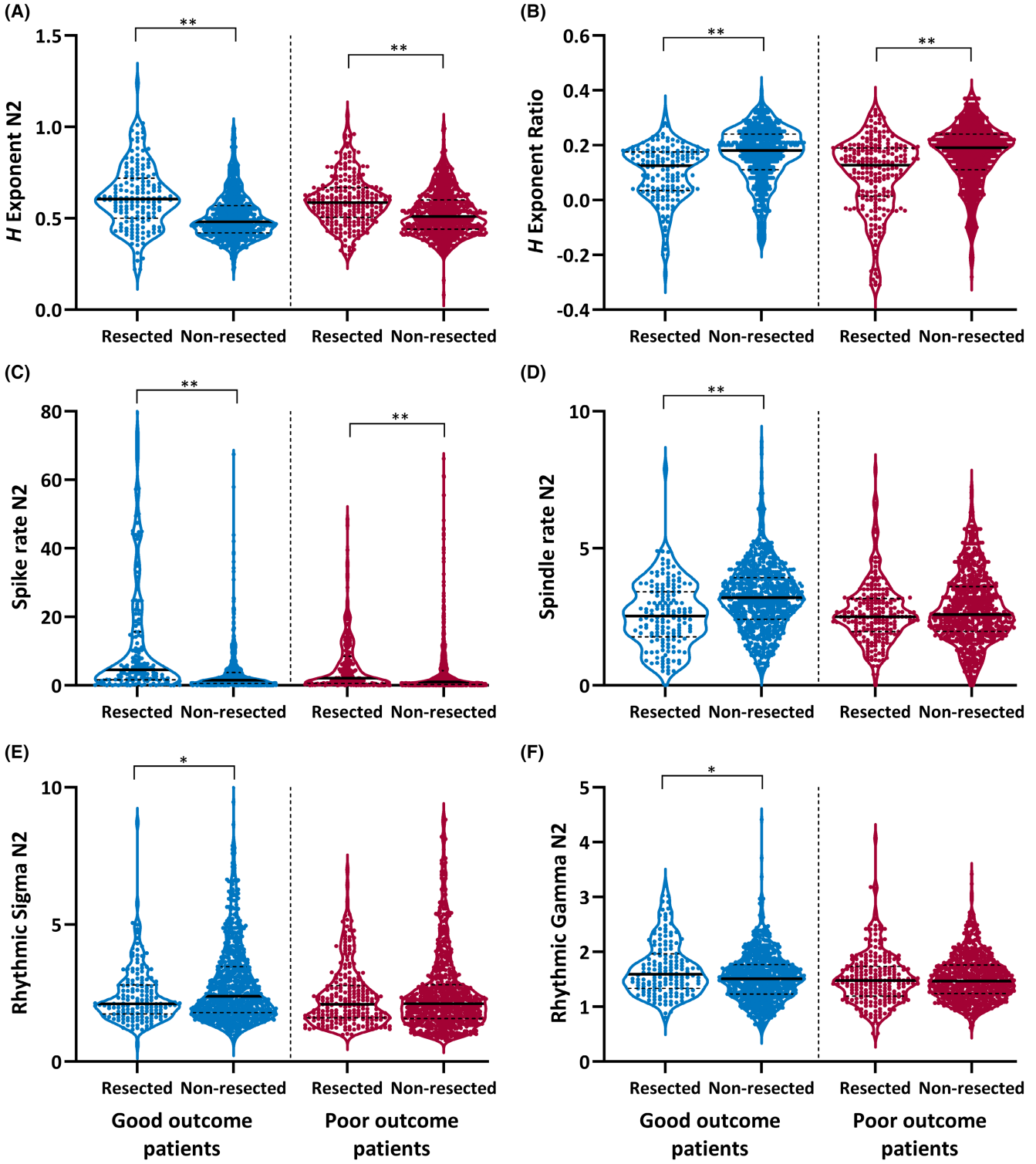

FIGURE 5 Oscillatory and nonoscillatory metrics during sleep in the resected and nonresected channels among good and poor outcome patients. Mann–Whitney *U*-tests revealed significant differences between the resected and nonresected channels for all sleep metrics in the good outcome patients. In the poor outcome patients, only the *H* exponent metrics and the spike rates differed among the resected and nonresected channels. Overall, effect sizes were largest in the good outcome patients, and were as follows (good, poor): (A) *H* exponent in N2 sleep (.28, .26), (B) *H* exponent ratio (.23, .26), (C) spike rates in N2 sleep (.26, .17), (D) spindle rates in N2 sleep (.21, .05), (E) rhythmic sigma in N2 sleep (.10, .009), and (F) rhythmic gamma in N2 sleep (.11, .002). $^{*}p < .01$, $^{**}p < .001$. Blue color represents good outcome patients, and red color represents poor outcome patients. Black thick lines in violin plots represent the median; dotted lines represent the quartiles.

lack of correlation between rhythmic sigma and spike rates might be related to the occurrence of spikes with ongoing rhythmic sigma power is unclear. Using conventional power spectral analysis on SEEG recordings of 10 children and adults with focal epilepsy, Zubler and colleagues[8] rather found a positive correlation between sigma power (12–16 Hz) and spike rates in the SOZ during NREM sleep, although this was significant in only seven of 10 subjects. Future research in larger patient samples is therefore needed to clarify the contribution of epilepsy processes to sigma spectral power, as measured traditionally as well as an isolated oscillatory component.

Second, we found a moderate influence of the epileptic network on rhythmic theta power, a reduction that was specific to N3 sleep and to the SOZ. This decrease in theta power was also associated with greater spiking activity in the SOZ. To our knowledge, this is a new finding that has not been reported previously in the literature. Hypothetically, these theta rhythms could be "replaced" by delta slowing in the context of lesional pathological brains, although this will need to be tested more thoroughly in future works. Third, at the other end of the spectrum, we observed an increase in rhythmic gamma power in the SOZ during NREM sleep. This oscillatory gamma power was not significantly correlated with the spike rate in the SOZ. Nevertheless, this increase in rhythmic gamma power is in agreement with recent works showing that higher NREM sleep gamma power[6] and epileptic spikes with preceding high-frequency activity (gamma 30–100 Hz[5] and ripple 80–500 Hz[42]) were among the best biomarkers for identifying the EZ in drug-resistant epilepsy patients. Whether the oscillatory gamma power—as examined here—performs differently than the more conventional gamma spectral measures, particularly when preceding an epileptic spike,[5] should be investigated in future research.

Surprisingly, the SW metrics could not distinguish the epileptic network. Although SW rates and rhythmic delta power tended to be lower in the SOZ relative to non-SOZ areas, these differences did not survive statistical correction for multiple comparisons. Given that spindles and SWs are thought to reflect healthy brain function, we expected that both graphoelements would be affected by epilepsy processes. Our findings rather suggest that spindles are particularly influenced by the epileptic network, in line with animal and human studies showing that epileptic activities can hijack mechanisms responsible for the generation of physiological spindles.[43]

4.2 | Nonoscillatory scale-free activity is altered within the epileptic network

Using a multifractal approach to study nonoscillatory brain activity, we show that the scale-free H exponent distinguished the SOZ from non-SOZ areas during N2 sleep. The H exponent was higher in the SOZ and IZ relative to the NZ, indicating a steeper $1/f$ slope. A higher H exponent in the SOZ was associated with a higher spike rate during N2 sleep. Our results also highlighted an abnormal scale-free behavior within the SOZ and IZ areas during N3 sleep, with the H exponent varying significantly less during deeper sleep stages. To quantify this difference, we computed a relative H exponent ratio of N3 over N2 sleep and found that ratios within the SOZ and IZ areas were closer to zero, indicating more steady $1/f$ slopes independently of increasing sleep depth.

Previous work using SEEG[20,21,44–46] and magnetoencephalographic recordings[47] found a higher H exponent during a seizure compared to seizure-free epochs. Although the neurophysiological underpinnings remain to be elucidated, it is hypothesized based on animal data that scale-free metrics may quantify neuronal excitability, with greater values indicating reduced neuronal excitatory–inhibitory balance (increased inhibition) in a given brain region.[13,15] Epileptogenic networks are suggested to be supercritical[48]; the occurrence of seizure activity disrupts this excitatory–inhibitory balance (excitability increases) and the brain's dynamics exhibit more persistent patterns, which is reflected by an increase in the H exponent. Our data add to these findings by suggesting that interictally, the epileptic network (SOZ) would be characterized by increased inhibition relative to non-SOZ areas. Additionally, it was previously shown that scale-free metrics vary with vigilance states, including sleep, with a higher H exponent as sleep depth increases.[49] Using the H exponent ratio, we observed the opposite trend; the SOZ behaves similarly despite increasing sleep depth. In light of this, our data indicate that the epileptic network would display an abnormally persistent signal (more similar inhibition levels) across interictal periods of N2 and N3 sleep.

Interestingly, our prediction model for identifying the resected channels in good outcome patients showed that the best features were the H exponent during N2 sleep and its N3/N2 ratio. These metrics had higher averaged BAC (.77 and .77) and AUC (.77 and .76) than the other sleep features. Their performance was as good as the SOZ (.76), used here as the clinical standard. Interestingly, in some patients (especially bilateral cases) where the SOZ performed poorly in identifying the resected channels, the H exponent metrics had higher sensitivity and specificity values. These findings support the proposal that nonoscillatory components of the neural signal can provide complementary information about the underlying pathological brain networks. Future work will be needed to test prospectively whether such scale-free metrics, in combination with other biomarkers, can accurately classify good

and poor outcome patients as well as delineate the EZ in larger patient cohorts.

This study has potential limitations, including the single-center design, with a moderate patient number ($n = 38$), of which 13 of 29 surgical patients had a good postsurgical outcome. Moreover, the use of SEEG recordings provides the unique opportunity to study neuronal activity from both deep structures and neocortical areas at a local and global scale, yet the implantation scheme is heterogeneous (patient-specific) and spatial resolution is limited to targeted brain areas. We also know from prior works that physiological spindles and SWs exhibit specific topographical patterns,[22,50] with lower rates in the medial temporal lobes, also frequent sites of epileptogenicity. Accounting for these potential confounding effects, we leveraged the availability of the Montreal Neurological Institute open iEEG Atlas[22] to quantify SEEG abnormalities across the brain in our patient sample by computing a patient-specific correction coefficient to obtain normalized feature values in epileptic areas.

ACKNOWLEDGMENTS

We wish to express our gratitude to the staff and technicians at the EEG Department of the Montreal Neurological Institute–Hospital, particularly Lorraine Allard, Nicole Drouin, and Chantal Lessard. This work was funded by a project grant from the Canadian Institutes of Health Research (PJT-175056) to B.F. B.F. was supported by Fonds de Recherche du Québec–Santé 2021–2023 Salary Award "Chercheur-Boursier Clinicien Senior." V.L. was supported by Banting Postdoctoral Fellowship 2020–2023.

CONFLICT OF INTEREST STATEMENT

None of the authors has any conflict of interest to disclose. We confirm that we have read the Journal's position on issues involved in ethical publication and affirm that this report is consistent with those guidelines.

DATA AVAILABILITY STATEMENT

Data that support the findings of this study are available from the corresponding author upon reasonable request.

ORCID

Véronique Latreille https://orcid.org/0000-0002-6431-9358
Laure Peter-Derex https://orcid.org/0000-0002-9938-9639
John Thomas https://orcid.org/0000-0003-0144-3746
Birgit Frauscher https://orcid.org/0000-0001-6064-1529

REFERENCES

1. Vakharia VN, Duncan JS, Witt JA, Elger CE, Staba R, Engel J. Getting the best outcomes from epilepsy surgery. Ann Neurol. 2018;83(4):676–90. https://doi.org/10.1002/ana.25205
2. Wiebe S, Jette N. Pharmacoresistance and the role of surgery in difficult to treat epilepsy. Nat Rev Neurol. 2012;8(12):669–77. https://doi.org/10.1038/nrneurol.2012.181
3. Rosenow F, Lüders H. Presurgical evaluation of epilepsy. Brain J Neurol. 2001;124(Pt 9):1683–700. https://doi.org/10.1093/brain/124.9.1683
4. Frauscher B. Localizing the epileptogenic zone. Curr Opin Neurol. 2020;33(2):198–206. https://doi.org/10.1097/WCO.0000000000000790
5. Thomas J, Kahane P, Abdallah C, Avigdor T, Zweiphenning WJEM, Chabardes S, et al. A subpopulation of spikes predicts successful epilepsy surgery outcome. Ann Neurol. 2022;93:522–35. https://doi.org/10.1002/ana.26548
6. Klimes P, Cimbalnik J, Brazdil M, Hall J, Dubeau F, Gotman J, et al. NREM sleep is the state of vigilance that best identifies the epileptogenic zone in the interictal electroencephalogram. Epilepsia. 2019;60(12):2404–15. https://doi.org/10.1111/epi.16377
7. Frauscher B, Von Ellenrieder N, Ferrari-Marinho T, Avoli M, Dubeau F, Gotman J. Facilitation of epileptic activity during sleep is mediated by high amplitude slow waves. Brain. 2015;138(6):1629–41. https://doi.org/10.1093/brain/awv073
8. Zubler F, Rubino A, Lo RG, Schindler K, Nobili L. Correlating interictal spikes with sigma and delta dynamics during non-rapid-eye-movement-sleep. Front Neurol. 2017;8(288):13–5. https://doi.org/10.3389/fneur.2017.00288
9. Nobili L, Ferrillo F, Baglietto MG, Beelke M, de Carli F, de Negri E, et al. Relationship of sleep interictal epileptiform discharges to sigma activity (12–16 Hz) in benign epilepsy of childhood with rolandic spikes. Clin Neurophysiol. 1999;110(1):39–46. https://doi.org/10.1016/S0168-5597(98)00041-0
10. Schiller K, Avigdor T, Abdallah C, Sziklas V, Crane J, Stefani A, et al. Focal epilepsy disrupts spindle structure and function. Sci Rep. 2022;12(1):11137. https://doi.org/10.1038/s41598-022-15147-0
11. Montplaisir J, Leduc L, Laverdiere M, Walsh J, Saint-Hilaire JM. Sleep spindles in the human hippocampus: normal or epileptic activity? Sleep. 1981;4(4):423–8. https://doi.org/10.1093/sleep/4.4.423
12. Frauscher B, Bernasconi N, Caldairou B, von Ellenrieder N, Bernasconi A, Gotman J, et al. Interictal hippocampal spiking influences the occurrence of hippocampal sleep spindles. Sleep. 2015;38(12):1927–33. https://doi.org/10.5665/sleep.5242
13. Gao R, Peterson EJ, Voytek B. Inferring synaptic excitation/inhibition balance from field potentials. NeuroImage. 2017;158:70–8. https://doi.org/10.1016/j.neuroimage.2017.06.078
14. Bröhl T, Rings T, Pukropski J, von Wrede R, Lehnertz K. The time-evolving epileptic brain network: concepts, definitions, accomplishments, perspectives. Front Netw Physiol. 2024;3:1338864. https://doi.org/10.3389/fnetp.2023.1338864
15. He BJ, Zempel JM, Snyder AZ, Raichle ME. The temporal structures and functional significance of scale-free brain activity. Neuron. 2010;66(3):353–69. https://doi.org/10.1016/j.neuron.2010.04.020
16. Pani SM, Fraschini M, Figorilli M, Tamburrino L, Ferri R, Puligheddu M. Sleep-related hypermotor epilepsy and non-rapid eye movement parasomnias: differences in the periodic and aperiodic component of the electroencephalographic power spectra. J Sleep Res. 2021;30:e13339. https://doi.org/10.1111/jsr.13339

17. van Heumen S, Moreau JT, Simard-Tremblay E, Albrecht S, Dudley RWR, Baillet S. Case report: aperiodic fluctuations of neural activity in the ictal MEG of a child with drug-resistant fronto-temporal epilepsy. Front Hum Neurosci. 2021;15:101. https://doi.org/10.3389/fnhum.2021.646426
18. Jiang H, Kokkinos V, Ye S, Urban A, Bagić A, Richardson M, et al. Interictal SEEG resting-state connectivity localizes the seizure onset zone and predicts seizure outcome. Adv Sci. 2022;9(18):2200887. https://doi.org/10.1002/advs.202200887
19. Barreto Mesquita V, Mendes Oliveira Filho F, Rodrigues PC. Detection of crossover points in detrended fluctuation analysis: an application to EEG signals of patients with epilepsy. Bioinformatics. 2021;37(9):1278–84. https://doi.org/10.1093/bioinformatics/btaa955
20. Janjarasjitt S. Spectral exponent characteristics of intracranial EEGs for epileptic seizure classification. IRBM. 2015;36:33–9. https://doi.org/10.1016/j.irbm.2014.07.005
21. Gadhoumi K, Gotman J, Lina JM. Scale invariance properties of intracerebral eeg improve seizure prediction in mesial temporal lobe epilepsy. PLoS One. 2015;10(4):1–23. https://doi.org/10.1371/journal.pone.0121182
22. von Ellenrieder N, Gotman J, Zelmann R, Rogers C, Nguyen DK, Kahane P, et al. How the human brain sleeps: direct cortical recordings of normal brain activity. Ann Neurol. 2020;87(2):289–301. https://doi.org/10.1002/ana.25651
23. Landman B, Warfield S. MICCAI 2012 workshop on multi-atlas labeling. MICCAI grand challenge and workshop on multi-atlas labeling. Nice, France: CreateSpace Independent Publishing Platform; 2012.
24. Drouin S, Kochanowska A, Kersten-Oertel M, Gerard IJ, Zelmann R, de Nigris D, et al. IBIS: an OR ready open-source platform for image-guided neurosurgery. Int J Comput Assist Radiol Surg. 2017;12(3):363–78. https://doi.org/10.1007/s11548-016-1478-0
25. Riedner BA, Vyazovskiy VV, Huber R, Massimini M, Esser S, Murphy M, et al. Sleep homeostasis and cortical synchronization: III. A high-density EEG study of sleep slow waves in humans. Sleep. 2007;30(12):1643–57. https://doi.org/10.1093/sleep/30.12.1643
26. Spanedda F, Cendes F, Gotman J. Relations between EEG seizure morphology, interhemispheric spread, and mesial temporal atrophy in bitemporal epilepsy. Epilepsia. 1997;38(12):1300–14. https://doi.org/10.1111/j.1528-1157.1997.tb00068.x
27. Engel J Jr, Van Ness P, Rasmussen T, Ojemann L. Outcome with respect to epileptic seizures. In: Engel J Jr, editor. Surgical Treatment of the Epilepsies. New York: Raven Press; 1993. p. 609–21.
28. Wieser HG, Blume WT, Fish D, Goldensohn E, Hufnagel A, King D, et al. Proposal for a new classification of outcome with respect to epileptic seizures following epilepsy surgery. Epilepsia. 2001;42(2):282–6. https://doi.org/10.1046/j.1528-1157.2001.35100.x
29. Janca R, Jezdik P, Cmejla R, Tomasek M, Worrell GA, Stead M, et al. Detection of interictal epileptiform discharges using signal envelope distribution modelling: application to epileptic and non-epileptic intracranial recordings. Brain Topogr. 2014;28(1):172–83. https://doi.org/10.1007/s10548-014-0379-1
30. Peter-Derex L, Klimes P, Latreille V, Bouhadoun S, Dubeau F, Frauscher B. Sleep disruption in epilepsy: ictal and interictal epileptic activity matter. Ann Neurol. 2020;88(5):907–20. https://doi.org/10.1002/ana.25884
31. Klimes P, Peter-Derex L, Hall J, Dubeau F, Frauscher B. Spatio-temporal spike dynamics predict surgical outcome in adult focal epilepsy. Clin Neurophysiol. 2022;134:88–99. https://doi.org/10.1016/j.clinph.2021.10.023
32. Andrillon T, Nir Y, Staba RJ, Ferrarelli F, Cirelli C, Tononi G, et al. Sleep spindles in humans: insights from intracranial EEG and unit recordings. J Neurosci. 2011;31(49):17821–34. https://doi.org/10.1523/JNEUROSCI.2604-11.2011
33. Mölle M, Marshall L, Gais S, Born J. Grouping of spindle activity during slow oscillations in human non-rapid eye movement sleep. J Neurosci. 2002;22(24):10941–47. https://doi.org/10.1523/JNEUROSCI.22-24-10941.2002
34. von Ellenrieder N, Frauscher B, Dubeau F, Gotman J. Interaction with slow waves during sleep improves discrimination of physiologic and pathologic high-frequency oscillations (80-500 Hz). Epilepsia. 2016;57(6):869–78. https://doi.org/10.1111/epi.13380
35. Wendt H, Abry P, Jaffard S. Bootstrap for empirical multifractal analysis. IEEE Signal Process Mag. 2007;24(4):38–48. https://doi.org/10.1109/MSP.2007.4286563
36. Wendt H, Abry P. Multifractality tests using bootstrapped wavelet leaders. IEEE Trans Signal Process. 2007;55(10):4811–20. https://doi.org/10.1109/TSP.2007.896269
37. Bernabei JM, Li A, Revell AY, Smith RJ, Gunnarsdottir KM, Ong IZ, et al. Quantitative approaches to guide epilepsy surgery from intracranial EEG. Brain. 2023;146(6):2248–58. https://doi.org/10.1093/brain/awad007
38. Bernabei JM, Sinha N, Arnold TC, Conrad E, Ong I, Pattnaik AR, et al. Normative intracranial EEG maps epileptogenic tissues in focal epilepsy. Brain J Neurol. 2022;145(6):1949–61. https://doi.org/10.1093/brain/awab480
39. Taylor PN, Papasavvas CA, Owen TW, Schroeder GM, Hutchings FE, Chowdhury FA, et al. Normative brain mapping of interictal intracranial EEG to localize epileptogenic tissue. Brain J Neurol. 2022;145(3):939–49. https://doi.org/10.1093/brain/awab380
40. Felice AD, Arcaro C, Storti SF, Fiaschi A, Manganotti P. Slow spindles' cortical generators overlap with the epileptogenic zone in temporal epileptic patients: an electrical source imaging study. Clin Neurophysiol. 2013;9:e193.
41. Clemens B, Ménes A. Sleep spindle asymmetry in epileptic patients. Clin Neurophysiol. 2000;111(12):2155–9. https://doi.org/10.1016/S1388-2457(00)00482-X
42. Shi W, Shaw D, Walsh KG, Han X, Eden UT, Richardson RM, et al. Spike ripples localize the epileptogenic zone best: an international intracranial study. Brain. 2024;147:2496–506. https://doi.org/10.1093/brain/awae037
43. Bernard C, Frauscher B, Gelinas J, Timofeev I. Sleep, oscillations, and epilepsy. Epilepsia. 2023;64(S3):S3–S12. https://doi.org/10.1111/epi.17664
44. Janjarasjitt S, Loparo KA. Examination of scale-invariant characteristics of multi-channel ECoG data for epileptic seizure localization. J Med Biol Eng. 2015;35(2):278–84. https://doi.org/10.1007/s40846-015-0020-0
45. Indiradevi KP, Elias E, Sathidevi PS. Complexity analysis of electroencephalogram records of epileptic patients using Hurst exponent. Int J Med Eng Inform. 2009;1(3):368–80. https://doi.org/10.1504/IJMEI.2009.022647

46. Yan J, Wang Y, Ouyang G, Yu T, Li Y, Sik A, et al. Analysis of electrocorticogram in epilepsy patients in terms of criticality. Nonlinear Dyn. 2016;83(4):1909–17. https://doi.org/10.1007/s11071-015-2455-9
47. Witton C, Sergeyev SV, Turitsyna EG, Furlong PL, Seri S, Brookes M, et al. Rogue bioelectrical waves in the brain: the Hurst exponent as a potential measure for presurgical mapping in epilepsy. J Neural Eng. 2019;16(5):056019. https://doi.org/10.1088/1741-2552/ab225e
48. Zimmern V. Why brain criticality is clinically relevant: a scoping review. Front Neural Circuits. 2020;14:54. https://doi.org/10.3389/fncir.2020.00054
49. Weiss B, Clemens Z, Bódizs R, Vágó Z, Halász P. Spatio-temporal analysis of monofractal and multifractal properties of the human sleep EEG. J Neurosci Methods. 2009;185(1):116–24. https://doi.org/10.1016/j.jneumeth.2009.07.027
50. Nir Y, Staba RJ, Andrillon T, Vyazovskiy VV, Cirelli C, Fried I, et al. Regional slow waves and spindles in human sleep. Neuron. 2011;70(1):153–69. https://doi.org/10.1016/j.neuron.2011.02.043

SUPPORTING INFORMATION

Additional supporting information can be found online in the Supporting Information section at the end of this article.

How to cite this article: Latreille V, Corbin-Lapointe J, Peter-Derex L, Thomas J, Lina J-M, Frauscher B. Oscillatory and nonoscillatory sleep electroencephalographic biomarkers of the epileptic network. Epilepsia. 2024;65:3038–3051. https://doi.org/10.1111/epi.18088